JACS
JOURNAL OF THE AMERICAN CHEMICAL SOCIETY

ARTICLE

pubs.acs.org/JACS

# Controlling Electron Trap Depth To Enhance Optical Properties of Persistent Luminescence Nanoparticles for In Vivo Imaging

Thomas Maldiney,[†] Aurélie Lecointre,[‡] Bruno Viana,[*,‡] Aurélie Bessière,[‡] Michel Bessodes,[†] Didier Gourier,[‡] Cyrille Richard,[*,†] and Daniel Scherman[†]

[†]Unité de Pharmacologie Chimique et Génétique et d'Imagerie, CNRS, UMR 8151, Paris, F-75270 cedex France, Inserm, U1022, Paris, F-75270 cedex France, Faculté des Sciences Pharmaceutiques et Biologiques, Université Paris Descartes, Paris, F-75270 cedex France, and ENSCP, Chimie ParisTech, Paris, F-75231 cedex France

[‡]Laboratoire de Chimie de la Matière Condensée de Paris, Ecole Nationale Supérieure de Chimie de Paris (Chimie ParisTech), CNRS, UMR 7574, Paris, 75231 cedex 05, France

Supporting Information

**ABSTRACT:** Focusing on the use of nanophosphors for in vivo imaging and diagnosis applications, we used thermally stimulated luminescence (TSL) measurements to study the influence of trivalent lanthanide $Ln^{3+}$ (Ln = Dy, Pr, Ce, Nd) electron traps on the optical properties of $Mn^{2+}$-doped diopside-based persistent luminescence nanoparticles. This work reveals that $Pr^{3+}$ is the most suitable $Ln^{3+}$ electron trap in the diopside lattice, providing optimal trap depth for room temperature afterglow and resulting in the most intense luminescence decay curve after X-ray irradiation. This luminescence dependency toward the electron trap is maintained through additional doping with $Eu^{2+}$, allowing UV-light excitation, critical for bioimaging applications in living animals. We finally identify a novel composition ($CaMgSi_2O_6$:$Eu^{2+}$,$Mn^{2+}$,$Pr^{3+}$) for in vivo imaging, displaying a strong near-infrared afterglow centered on 685 nm, and present evidence that intravenous injection of such persistent luminescence nanoparticles in mice allows not only improved but highly sensitive detection through living tissues.

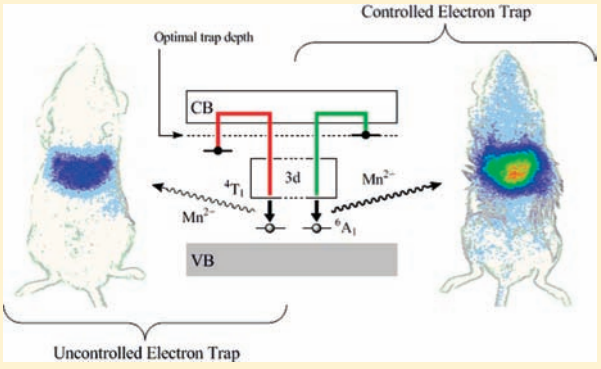


## INTRODUCTION

In vivo optical imaging, using photons as primary information, has witnessed several major improvements in the last decades.[1] Among a wide panel of very sensitive and efficient photonic probes, inorganic-based sensors, such as quantum dots (QDs), potentially offer the highest quantum efficiency through living tissue.[2] Yet genuinely intense, QDs emission requires continuous illumination and thereby suffers from significant background signal (autofluorescence) emitted from irradiated tissues.[3]

To address this important issue, we reported the synthesis of persistent luminescence nanoparticles (PLNP) with the formula $Ca_{0.2}Zn_{0.9}Mg_{0.9}Si_2O_6$:$Eu^{2+}$,$Mn^{2+}$,$Dy^{3+}$ (hereafter referred to as CZMSO:Eu,Dy) and sharing the same crystalline structure as diopside $CaMgSi_2O_6$.[4] Such material possesses the ability to be excited under UV light before intravenous injection in mice, and to emit in the near-infrared window without further irradiation, circumventing autofluorescence from animal tissues. We have shown that PLNP could be used as a sensitive optical probe for in vivo imaging, and that their biodistribution was highly dependent on both core diameter and global surface charge.[5] However, luminescence from these PLNP was not intense enough to provide long-term monitoring of in vivo probe accumulation, unveiling the need to work on new nanomaterials with improved optical characteristics.

To better understand the origin of such a phenomenon in the CZMSO lattice, and to ensure pure diopside crystalline structure, we have previously suggested a mechanism of persistent luminescence in the diopside host, with $Mn^{2+}$ acting both as the hole trap and the recombination center. The X-ray induced thermally stimulated luminescence (TSL) measurements revealed that when $Dy^{3+}$ was added as a codoping ion, the red persistent luminescence was enhanced.[6] We then hypothesized that trivalent lanthanide ions could act as an efficient electron trap for persistent luminescence.[7]

Starting from the hypothesis that controlling electrons trap depth could help to enhance the optical properties of PLNP,[8] we presently report the synthesis of several $Mn^{2+}$ doped diopside nanoparticles, either codoped with trivalent lanthanide ions $CaMgSi_2O_6$:$Mn^{2+}$,$Ln^{3+}$ (Ln = Dy, Pr, Ce, Nd), only excitable with X-rays (hereafter referred to as CMSO:Ln), or tridoped with divalent europium and trivalent lanthanide ions $CaMgSi_2O_6$:$Mn^{2+}$,$Eu^{2+}$,$Ln^{3+}$, to enable UV excitation (hereafter referred to as CMSO:Eu,Ln). These nanomaterials were compared to hybrid enstatite−diopside CZMSO already used for in vivo imaging. Divalent manganese, present in all the compounds, is at

**Received:** May 25, 2011
**Published:** June 24, 2011

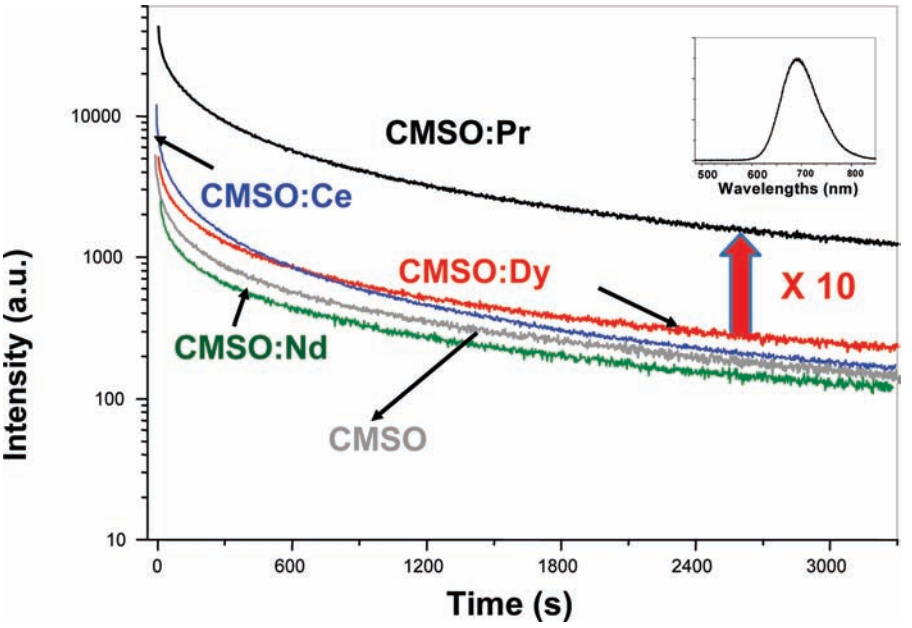


**Figure 1.** Decay of the $Mn^{2+}$ luminescence intensity at 685 nm of CMSO and rare-earth-codoped CMSO:Ln compounds, recorded after 10 min X-ray irradiation. Insert: LLP spectrum, 6 s after X-ray irradiation, due to the $^4T_1 \rightarrow {}^6A_1$ transition of $Mn^{2+}$ ions in the $Mg^{2+}$ sites.

the origin of the red emission (transition from $^4T_1$ to the fundamental $^6A_1$ manifold).[6] In this work, we identify $Pr^{3+}$ as the optimal electron trap in the diopside host, which led to an improved nanomaterial, excitable with UV light and displaying the most intense afterglow in the near-infrared region. We finally managed to extract nanoparticles with narrow distribution from the initial polydispersed powder and report their application for highly sensitive real-time in vivo bioimaging in mice.

## RESULTS AND DISCUSSION

**Sol−Gel Synthesis of Diopside Nanoparticles and X-ray Diffraction (XRD) Characterization.** Inorganic phosphors are generally synthesized by solid-state reaction, leading to micrometer-sized particles, unsuitable for in vivo experiments.[9,10] For this reason, we preferred a sol−gel processing[11] under acidic conditions that allows a lower calcination temperature and provides nanocrystalline materials. The XRD patterns of CMSO:Eu, Pr and CMSO:Eu,Dy, shown in Figure S1 (Supporting Information), confirm the formation of pure monoclinic diopside crystallizing with space group $C2/c$ (JCPDS file No. 78-1390). Similar patterns were observed for CMSO:Dy, CMSO:Pr, CMSO:Ce, and CMSO:Nd. Hybrid hosts CZMSO:Eu,Pr and CZMSO:Eu,Dy also displayed the diopside pattern, but with broadened peaks, certainly due to the presence of enstatite residual phase (data not shown). Besides, we noticed that switching trivalent lanthanide or adding divalent europium as an extra dopant has no significant effect on the global structure of our final products.

**Optical Characteristics of $Mn^{2+}$ in the Diopside Host.** Photoluminescence excitation and emission spectra, displayed in Supporting Information (Figure S2), show that near-infrared optical properties of tridoped CMSO:Eu,Pr are very similar to those previously observed in tridoped CZMSO:Eu,Dy.[4] The same characteristics were observed for each synthesized compound (data not shown). All diopside nanomaterials display several broad excitation bands between 270 and 420 nm due to 4f-5d transitions of $Eu^{2+}$. The emission spectra are composed of two emission bands at 580 and 685 nm. These bands are similar to those observed for diopsides doped only with $Mn^{2+}$ and correspond to the same $^4T_1 \rightarrow {}^6A_1$ transition of $Mn^{2+}$ in two different surroundings.[7] $Mn^{2+}$ in the $Mg^{2+}$ site is responsible for the 685 nm emission band, whereas $Mn^{2+}$ in the $Ca^{2+}$ site leads to the 580 nm emission band.

Interestingly, we notice from the long-lasting phosphorescence (LLP) spectrum (insert in Figure 1) that emission from $Mn^{2+}$ in the $Ca^{2+}$ site has disappeared, resulting in a characteristic and exclusive red persistent luminescence around 685 nm due to $Mn^{2+}$ in the $Mg^{2+}$ site, which is very suitable for in vivo applications.[12]

**Controlling Electron Trap Depth in CMSO:Ln Nanoparticles.** Taking into account the results from X-ray-induced TSL measurements in the CMSO host, we have previously hypothesized that $Mn^{2+}$ acts both as recombination center and hole trap.[7] The efficiency of persistent luminescence is determined by thermally activated detrapping of electrons. Moreover, preliminary experiments on $Dy^{3+}$- and $Mn^{2+}$-codoped diopside (referred to here as CMSO:Dy) suggested that the rare earth ion is an electron trap.[7] Owing to the variation of electron affinity and ionization energy along the lanthanide ($Ln^{3+}$) series, we may expect to control the electron trap depth by specific $Ln^{3+}$ doping.[13,14] Figure 1 shows the persistent afterglow at 685 nm following X-ray excitation of CMSO (only doped with manganese) and CMSO:Ln with Ln = $Dy^{3+}$, $Pr^{3+}$, $Ce^{3+}$, and $Nd^{3+}$. It appears that CMSO, CMSO:Dy, CMSO:Ce, and CMSO:Nd matrixes exhibit similar long-lasting phosphorescence (LLP), while CMSO:Pr shows a 10 times increased emission intensity with the same nonexponential decay kinetics.

This luminescence enhancement by $Pr^{3+}$ doping can be understood by comparing TSL spectra of the different CMSO matrixes, shown in Figure 2. The dashed rectangle represents the approximate temperature range where electron traps contribute

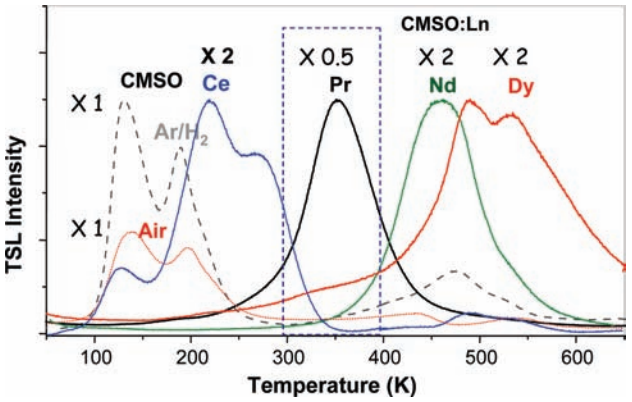


**Figure 2.** $Mn^{2+}$ TSL intensity at 685 nm of CMSO and CMSO:Ln materials, recorded after 10 min X-ray irradiation. The approximate temperature range of interest for room temperature persistent luminescence is delimited by a dotted rectangle. The dotted curve (in red) and the interrupted curve (in black) represent TSL of CMSO treated at 1100 °C in air and in $Ar/H_2$ atmosphere, respectively. The other curves represent TSL of CMSO:Ln, with 1% doping with Ln = $Ce^{3+}$, $Nd^{3+}$, $Dy^{3+}$, and $Pr^{3+}$. Except for the case of CMSO treated in air, all the TSL curves are normalized to that of CMSO treated in $Ar/H_2$, with the amplification (or reduction) coefficients given in the figure.

to the room temperature afterglow. Uncodoped CMSO (i.e., only doped with 2.5% $Mn^{2+}$) sintered at 1100 °C for 10 h in air and in a reducing $Ar/H_2$ atmosphere gives the red dotted curve and the discontinuous black glow curve, respectively. One observes intense TSL peaks at 130 K and 190 K, and weaker peaks above room temperature due to intrinsic defects acting as electron traps. Low temperature peaks are twice enhanced in CMSO thermally annealed under reducing conditions, and a new and intense peak appears at 475 K. Therefore, reducing conditions favor the formation of intrinsic defects, and the new peak at 475 K is likely due to oxygen vacancies,[15,16] known as efficient electron traps.

The situation where TSL peaks are located far below and far above room temperature is not optimal for a strong LLP, as the low temperature peaks only contribute to the short time part of the afterglow, while thermal energy at room temperature is not sufficient to induce a significant electron release from deep traps, which control the intensity and the length of the afterglow.

The TSL signal is strongly modified upon doping with trivalent rare earth ions (Figure 2), with new peaks in a broad temperature range, replacing the low temperature peaks at 130 K and 190 K. This confirms that $Ln^{3+}$ ions act as electron traps and that their depth can be tuned by changing the trivalent lanthanide. The TSL peaks of $Nd^{3+}$ (460 K) and $Dy^{3+}$ (480 K and 530 K) are in the same temperature range as oxygen vacancy intrinsic defects (475 K). This explains why $Nd^{3+}$ and $Dy^{3+}$ doping have little effect on the intensity and length of the afterglow. The TSL glow curve of CMSO:Ce is more complex, with a low temperature peak (≈130 K) similar to the undoped material, and two peaks at higher temperatures (216 K and 270 K). However, the latter are still below room temperature so they do not influence the intensity and length of the afterglow. On the contrary, $Pr^{3+}$ gives a very strong TSL peak centered at 353 K (see the normalizing coefficient for the different $Ln^{3+}$ cations in Figure 2). The position of this TSL peak just above room temperature explains why an intense and long-lasting luminescence is observed for CMSO:Pr. The high intensity of

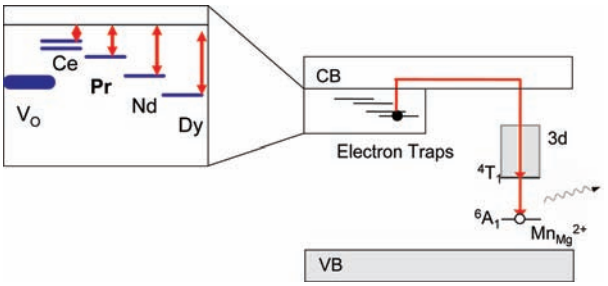


**Figure 3.** Schematic energy level diagram of $Mn^{2+}$ and $Ln^{3+}$ in CMSO. The main hole traps are $Mn^{2+}$ ions in the $Mg^{2+}$ site, while electrons are trapped by oxygen vacancies ($V_O$) and $Ln^{3+}$ ions. TSL and persistent luminescence occur by thermally activated electron release and capture by $Mn^{3+}$ ions, giving the $Mn^{2+}$ emission. The insert shows the relative positions of electron trap levels with respect to the conduction band edge.

the TSL peak of CMSO:Pr compared to CMSO:Nd and CMSO:Dy by a factor close to 4 may be partly due to the thermal quenching of $Mn^{2+}$ luminescence when going from room temperature to higher temperature.

The mechanism of TSL and long lasting luminescence is summarized in Figure 3, which displays a schematic energy level diagram of $Mn^{2+}$- and $Ln^{3+}$-doped CMSO. During irradiation, holes are mainly trapped by $Mn^{2+}$ ions in $Mg^{2+}$ sites,[7] giving $Mn^{3+}$, while electrons are trapped by oxygen vacancies and $Ln^{3+}$ ions. Upon thermal activation, electrons are released from their traps and captured by $Mn^{3+}$, giving rise to the $^4T_1 \rightarrow {}^6A_1$ $Mn^{2+}$ emission. The different trap depths $E$ (with respect to the conduction band edge) can be roughly estimated by the simple expression[17] $E \approx 0.002T_M$, where $T_M$ is the temperature of the peak maximum. It gives $E \approx 0.95$ eV for the oxygen vacancies ($T_M = 475$ K), and $E \approx 0.4$ and 0.5 eV ($Ce^{3+}$), $E \approx 0.7$ eV ($Pr^{3+}$), $E \approx 0.92$ eV ($Nd^{3+}$), and $E \approx 0.96-1$ eV ($Dy^{3+}$). It thus appears that an electron trap depth of about 0.7 eV is a good compromise for a strong room temperature long-lasting luminescence in diopside.

**UV-Induced Persistent Luminescence in CMSO:Eu,Ln Nanoparticles.** We have seen that persistent luminescence occurs in CMSO:Ln and that controlling electron trap depth could lead to more efficient materials with intense persistent luminescence properties. However, X-ray irradiation hampers further use of these materials for in vivo imaging. Thereby, in order to afford practical application, divalent europium was used as an extra dopant for sensitization to UV irradiation. Persistent luminescence decay was followed under the photon counting system after 5 min UV excitation. Figure 4 shows the decay curves for CMSO:Eu,Dy and CMSO:Eu,Pr nanoparticles compared to our previous silicate CZMSO:Eu,Dy, described as the first long-lasting luminescence material for real-time bioimaging,[4] as well as CZMSO:Eu,Pr. The afterglow dependency, witnessed with X-ray excitable bidoped compounds, is preserved after additional doping with divalent europium. Indeed, $Pr^{3+}$ still acts as the most efficient electron trap for persistent luminescence, leading to a CMSO:Eu,Pr emission more than 100 times brighter than in the case of CMSO:Eu,Dy. Interestingly, the factor 10 that kept apart both CMSO:Dy and CMSO:Pr after X-ray excitation transforms into a factor superior to 100 in europium-doped CMSO:Eu,Dy and CMSO:Eu,Pr after UV excitation. This amplification of the difference between Dy- and Pr-doped materials can be explained from the role of europium, required

to capture UV photons (there is no persistent luminescence under UV excitation without $Eu^{2+}$ doping), as $Ln^{3+}$ ions are localized close to $Eu^{2+}$ ions, which decreases the competition with other electron traps. Yet, the most promising result comes from the comparison of the new CMSO:Eu,Pr nanoparticles to the first generation of CZMSO:Eu,Dy nanoparticles.[4] Experimental results in Figure 4 show that the red luminescence from CMSO:Eu,Pr appears about 7 times more intense than that in the previously described $Ca_{0.2}Zn_{0.9}Mg_{0.9}Si_2O_6:Eu^{2+},Mn^{2+},Dy^{3+}$ (CZMSO:Eu,Dy) NPs. We notice that $Pr^{3+}$ failed to increase the afterglow in hybrid CZMSO host, comprising both enstatite and diopside. Although $Pr^{3+}$ seems to be the optimal electron trap in diopside, this trend has no reason to be maintained in a different silicate host, enstatite in particular. Indeed, TSL measurements (not shown) show that the peaks at 480 K and 530 K of CMSO:Dy are weaker, broader, and shifted to 330 K and 475 K in CZMSO:Dy, which corresponds to electron trap depths of 0.66 and 0.95 eV, respectively. As a trap depth of ≈0.7 eV is optimal for an optimized long-lasting luminescence, this result indicates that dysprosium act as a better electron trap in enstatite than praseodymium, while the contrary holds for diopside.

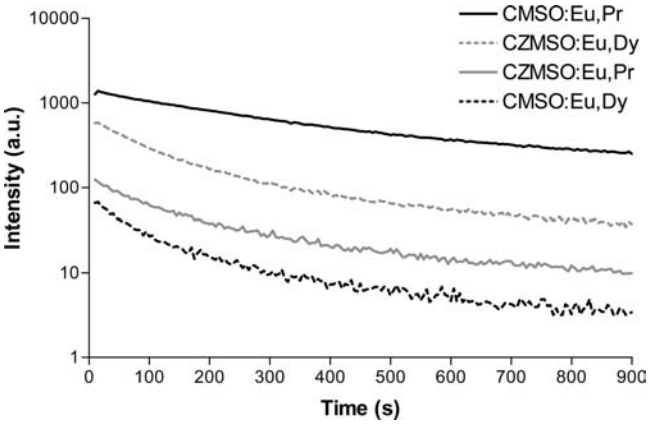


**Figure 4.** Decay of the persistent luminescence of CZMSO:Eu,Dy, CZMSO:Eu,Pr, CMSO:Eu,Dy, and CMSO:Eu,Pr compounds recorded after 5 min UV excitation (6 W lamp, 254 nm) with the Biospace Photon-Imager (for each composition, we used 10 mg of powder).

In order to validate a potential use of this new efficient composition for in vivo imaging, we selected the best two candidates from polydisperse samples (CZMSO:Eu,Dy and CMSO:Eu,Pr) and confronted them with the exact same nanosized distribution for mice bioimaging.

**CZMSO- and CMSO-Based PLNP Characterization.** In a previous study, we have demonstrated that the intensity of persistent luminescence in diopside is not only dependent on the amount of material but also on the diameter of nanoparticles.[5] For this reason, it was critical to extract persistent luminescence nanoparticles (PLNP) with an identical size for each compound in order to compare their emission properties. As indicated in Supporting Information (Figure S3), particle size distribution (measured by dynamic light scattering) as well as transmission electron micrographs for CZMSO- and CMSO-based PLNP show that both types of PLNP display the same shape (not exact spheroids) and have the same hydrodynamic diameter of approximately 140 nm in aqueous solution. The persistent luminescence decay curves of crude PLNP suspended in normal saline solution (injection medium, 150 mM NaCl, pH = 5.5) were acquired for 15 min with a photon imager (Biospace, Paris, France). Results in Supporting Information (Figure S4) show that a significant difference is still noticeable between CZMSO and CMSO hosts after narrowing the nanoparticle size distribution. Nevertheless, calculated values emphasize a slight decrease in the ratio of intensities (CMSO compared to CZMSO), and the factor 7 observed for polydisperse nanomaterials turns into a factor 5 with the same nanoparticle distribution. This weak decrease in the ratio could be attributed to different surface-quenching effects, depending on the host structure, composition, or crystallization degree.[18,19]

**In Vivo Imaging.** A comparative in vivo study of the two best UV-excitable diopside-based compositions (CZMSO:Eu,Dy and CMSO:Eu,Pr) was therefore necessary in order to ensure a significant difference between selected luminescent nanoparticles through living animal tissues. Figure 5 shows the luminescence images obtained from the photon-counting system after

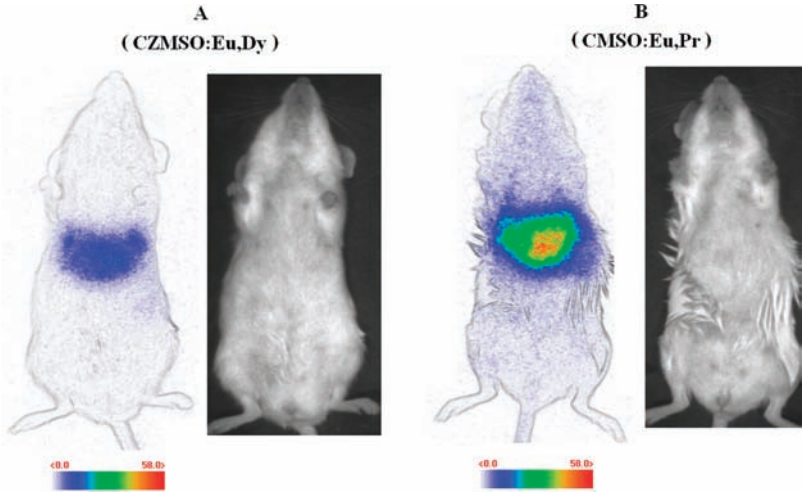


**Figure 5.** In vivo imaging of different CZMSO and CMSO diopside PLNPs under the photon-counting system. (A) CZMSO:Eu,Dy; (B) CMSO:Eu,Pr. The signal was recorded for 15 min following systemic injection of the probes (100 $\mu$g, excited 5 min under a 6 W UV lamp at 254 nm before injection). Luminescence intensity is expressed in false color units (1 unit = 2800 photons per s · $cm^2$ · steradians). For both compositions (A and B), the left picture represents the luminescence signal from PLNP, and the right picture represents the photograph of the imaged mouse.


dx.doi.org/10.1021/ja204504w |J. Am. Chem. Soc. 2011, 133, 11810–11815

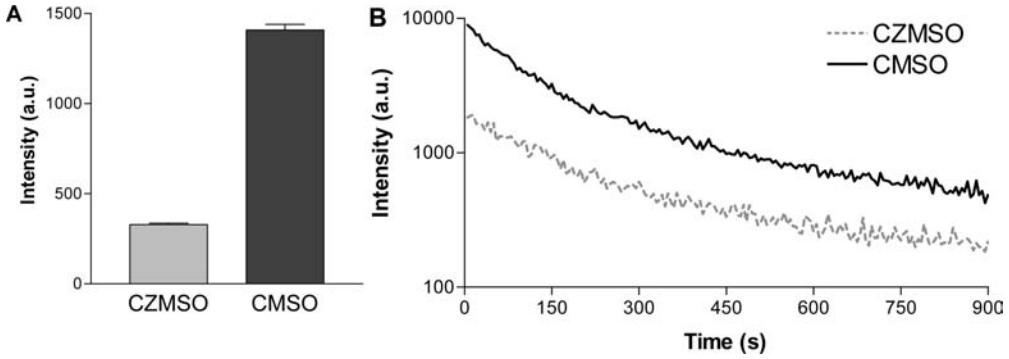


**Figure 6.** (A) Semiquantitative image-based comparison of the signals acquired after 1 min from the whole mouse body. (B) Comparative luminescence decay curves corresponding to the signal of each mouse.

15 min acquisition, as well as photographs of the imaged mice. Both compositions have the same biodistribution: PLNP almost instantly concentrates within the liver. This trend, already witnessed with many nanoparticle systems,[20] is mainly related to the global negative charge of the nanoprobes under physiological pH that triggers a recognition process via opsonins, leading to a major uptake of hydroxyl-PLNP by Kupffer cells in the liver. The difference between CZMSO:Eu,Dy- and CMSO:Eu,Pr-injected mice is striking. First, the new composition lightens some of the main pectoral limbs' circulation routes, indistinguishable on the CZMSO-injected mouse. Then, a closer look at the luminescence signals reveals a significant change in the surface delimited by equal intensities around liver. Indeed, after adjustment of threshold and appropriate binarization treatment, image analysis of the liver from mice A and B in the bottom of Figure S5 (Supporting Information) indicates that the ROI surface calculated from the PLNP signal in liver significantly increases from mouse A (injected with CZMSO:Eu,Dy) to mouse B (injected with CMSO:Eu,Pr). This result, obviously dependent on photon scattering by tissues, indicates that praseodymium-doped diopside (CMSO:Eu,Pr) returns additional information on PLNP in vivo local distribution within the liver, allowing a more sensitive detection of the probe through living tissues.

The Biospace photon-counting process allowed semiquantization of the signals from comparative study of PLNP in mice A and B. Results presented in Figure 6 indicate that CMSO:Eu,Pr is almost five times more intense through living tissues (Figure 6A). Despite a weak trend to decrease with time, this factor remains quite stable after several minutes (Figure 6B) and ensures an observation for longer periods of time (from 3 to 5 times longer). For example, the emission intensity for CMSO after 900 s is equivalent to that of CZMSO after only 200 s. This improvement should allow new applications for real-time in vivo imaging. Moreover, it shows an exciting perspective in the development of new targeting PLNP to visualize tumor environment, generally achievable through longer circulation of the probe. At last, although diopside appears very likely to be biocompatible,[21,22] the improved signal could be used to reduce injected dose and circumvent, or at least reduce, possible toxic effects to be expected after intravenous administration of silicate- and zinc-containing nanoprobes.

## CONCLUSION

We managed to control lanthanide electron trap depth to highly enhance the red-afterglow of this material. We found that doping CMSO with $Pr^{3+}$ ions provides electron trap levels about 0.7 eV below the conduction band edge, which allows optimal electron release and recombination at room temperature responsible for the highest persistent luminescence. Additional doping with divalent europium not only allowed UV excitation of PLNP, critical for a suitable in vivo application, but also left the relative efficiency of electron traps unchanged. Particle size selection and surface modification led to a novel near-infrared optical nanoprobe with high sensitivity and negative surface charge. We finally demonstrated the advantages of these intense in vivo PLNP, for real-time optical imaging in healthy mice, responsible for a significant signal benefit through living tissue and the ability to access longer monitoring of the probe.

## ASSOCIATED CONTENT

**Supporting Information.** XRD patterns, TEM images, optical properties, and size distributions of the injected nanoparticles, as well as image analysis results (from Image J software) after PLNP systemic injection in mice. This material is available free of charge via the Internet at http://pubs.acs.org.

## AUTHOR INFORMATION

**Corresponding Author**

cyrille.richard@parisdescartes.fr; bruno-viana@chimie-paristech.fr

## ACKNOWLEDGMENT

We thank René Lai Kuen, Bruno Saubaméa, and Johanne Seguin for their contribution and help to record transmission electron micrographs and perform in vivo experiments and image analysis with Image J software. This work has been supported by the French National Agency (ANR) in the frame of its program in Nanosciences and Nanotechnologies (NATLURIM project no. ANR-08-NANO-025).

## REFERENCES

(1) Weissleder, R.; Pittet, M. J. *Nature* **2008**, *452*, 580–589.
(2) Medintz, I. L.; Uyeda, H. T.; Goldman, E. R.; Mattoussi, H. *Nat. Mater.* **2005**, *4*, 435–446.
(3) Frangioni, J. V. *Curr. Opin. Chem. Biol.* **2003**, *7*, 626–634.
(4) le Masne de Chermont, Q.; Chanéac, C.; Seguin, J.; Pelle, F.; Maîtrejean, S.; Jolivet, J.-P.; Gourier, D.; Bessodes, M.; Scherman, D. *Proc. Natl. Acad. Sci. U.S.A.* **2007**, *104*, 9266–9271.

(5) Maldiney, T.; Richard, C.; Seguin, J.; Wattier, N.; Bessodes, M.; Scherman, D. *ACS Nano* **2011**, *5*, 854–862.
(6) Lecointre, A.; Viana, B.; LeMasne, Q.; Bessière, A.; Chanéac, C.; Gourier, D. *J. Lumin.* **2009**, *129*, 1527–1530.
(7) Lecointre, A.; Bessière, A.; Viana, B.; Gourier, D. *Radiat. Meas.* **2010**, *45*, 497–499.
(8) Lü, X.; Shu, W.; Fang, Q.; Yu, Q.; Xiong, X. *J. Mater. Sci.* **2007**, *42*, 6240–6245.
(9) *Phosphor Handbook*; Weber, M. J. Ed. CRC Press: Boca Raton, Boston, London, New York, Washington DC, 1999.
(10) Escribano, P.; Julian-Lopez, B.; Planelles-Arago, J.; Cordoncillo, E.; Viana, B.; Sanchez, C. *J. Mater. Chem.* **2008**, *18*, 23–40.
(11) Brinker, C. J.; Scherer, G. W. *The Physics and Chemistry of the Sol Gel Processing*; Academic: London, 1990.
(12) Cheong, W. J.; Prahl, S. A.; Welch, A. J. *IEEE J. Quantum Electron.* **1990**, *26*, 2166–2185.
(13) Lecointre, A.; Bessière, A.; Bos, A. J. J.; Dorenbos, P.; Viana, B.; Jacquart, S. *J. Phys. Chem. C* **2011**, *115*, 4217–4227.
(14) Dorenbos, P.; Krumpel, A. H.; van der Kolk, E.; Boutinaud, P.; Bettinelli, M.; Cavalli, E. *Opt. Mater.* **2010**, *32*, 1681–1685.
(15) Pauwels, D.; Le Masson, N.; Viana, B.; Kahn-Harari, A.; van Loef, E. V. D.; Dorenbos, P.; van Eijk, C. W. E. *IEEE Trans. Nucl. Sci.* **2000**, *47*, 1787–1790.
(16) Pidol, L.; Kahn-Harari, A.; Viana, B.; Virey, E.; Ferrand, B.; Dorenbos, P.; de Haas, J. T. M.; van Eijk, C. W. E. *IEEE Trans. Nucl. Sci.* **2004**, *51*, 1084–1087.
(17) Randall, J. T.; Wilkins, M. H. F. *Proc. R. Soc. A* **1945**, *184*, 366–389.
(18) Mialon, G.; Turkcan, S.; Alexandrou, A.; Gacoin, T.; Boilot, J. P. *J. Phys. Chem. C* **2009**, *113*, 18699–18706.
(19) Buissette, V.; Huignard, A.; Gacoin, T.; Boilot, J. P.; Aschehoug, P.; Viana, B. *Surf. Sci.* **2003**, *532*, 444–449.
(20) Kumar, R.; Roy, I.; Ohulchanskky, T. Y.; Vathy, L. A.; Bergey, E. J.; Sajjad, M.; Prasad, P. N. *ACS Nano* **2010**, *4*, 699–704.
(21) Nonami, T.; Tsutsumi, S. *J. Mater. Sci. Mater. Med.* **1999**, *10*, 475–479.
(22) Wu, C.; Chang, J. *J. Biomed. Mater. Res., Part B* **2007**, *83*, 153–160.